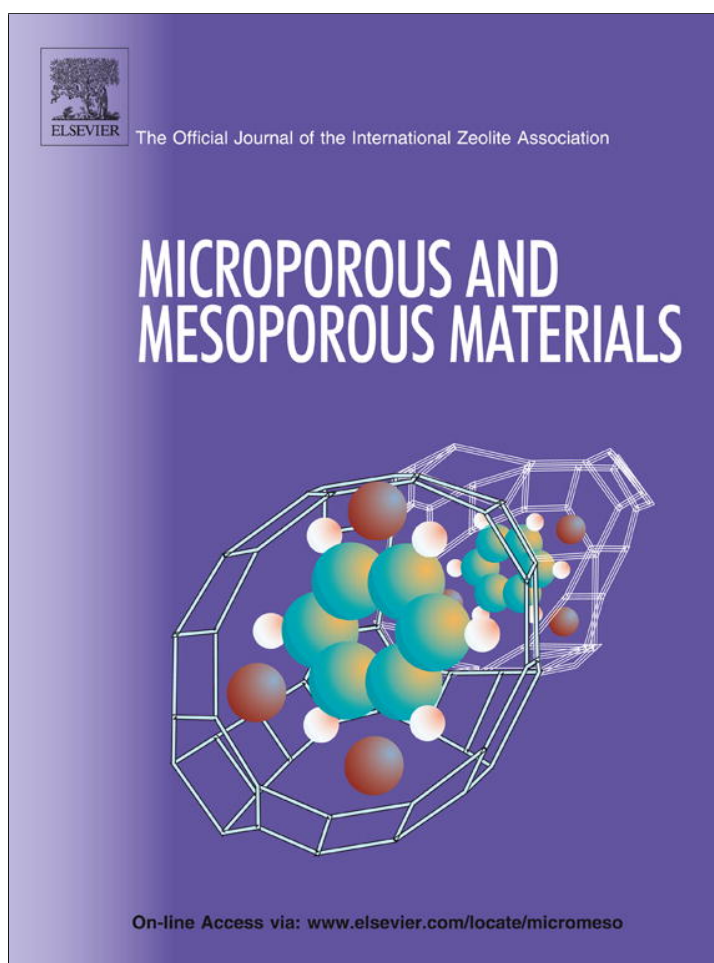


Provided for non-commercial research and education use.
Not for reproduction, distribution or commercial use.



This article appeared in a journal published by Elsevier. The attached copy is furnished to the author for internal non-commercial research and education use, including for instruction at the authors institution and sharing with colleagues.

Other uses, including reproduction and distribution, or selling or licensing copies, or posting to personal, institutional or third party websites are prohibited.

In most cases authors are permitted to post their version of the article (e.g. in Word or Tex form) to their personal website or institutional repository. Authors requiring further information regarding Elsevier's archiving and manuscript policies are encouraged to visit:

<http://www.elsevier.com/authorsrights>



Contents lists available at SciVerse ScienceDirect

Microporous and Mesoporous Materials

journal homepage: www.elsevier.com/locate/micromeso

Fabrication of two perovskite-type oxide nanoparticles as the new adsorbents in efficient removal of a pesticide from aqueous solutions: Kinetic, thermodynamic, and adsorption studies

Haman Tavakkoli^{a,*}, Mohammad Yazdanbakhsh^b^a Department of Chemistry, Science and Research Branch, Islamic Azad University, Khouzestan, Iran^b Department of Chemistry, Faculty of Science, Ferdowsi University of Mashhad, Mashhad, Iran

ARTICLE INFO

Article history:

Received 18 December 2012

Received in revised form 17 March 2013

Accepted 24 March 2013

Available online 6 April 2013

Keywords:

Nanostructures

Perovskite-type oxide

Adsorbent

Pesticide removal

Kinetic and thermodynamic study

ABSTRACT

The perovskite-type $\text{LaFe}_{0.9}\text{Co}_{0.1}\text{O}_3$ (LFCO1) and $\text{LaFe}_{0.1}\text{Co}_{0.9}\text{O}_3$ (LFCO2) nanoparticles (NPs) were prepared via sol–gel method. The structure and morphology of NPs were characterized by thermogravimetric analysis (TGA), X-ray diffraction (XRD), infrared spectroscopy (FT-IR), scanning electron microscopy (SEM), scanning tunneling microscopy (STM), energy dispersive X-ray spectroscopy (EDX), and Brunauer–Emmett–Teller (BET). The average particle size of NPs is approximately between 20 and 40 nm. The ability of calcined NPs to remove vitavax as a typical pesticide in aqueous solutions was assessed. The removal kinetic studies were conducted on LFCOs NPs with different contact time, temperatures, initial pesticide concentrations, and adsorbent doses to find the optimum conditions. The results showed both NPs can remove the vitavax from aqueous solution with a very high adsorption capacity. The removal process follows first-order kinetics and the Langmuir adsorption isotherm model. The activation energy and Arrhenius factor were obtained from temperature dependence of the rate constant. The thermodynamic parameters of the adsorption were also determined.

© 2013 Elsevier Inc. All rights reserved.

1. Introduction

The use of pesticides, which constitute a major class of hazardous compounds, has increased markedly in recent years due to their extensive applications in agriculture. In some developing and transitional countries, there are more than half a million tons of obsolete, unused, banned, or outdated pesticides which endanger the environment and the health of millions of people. In the absence of a clear strategy for obsolete pesticide management, significant amounts of obsolete pesticides have been stockpiled over the years in developing countries [1].

The contamination of surface and ground waters by pesticides is an important problem that scientists are dealing with for their effective elimination. The process of pesticide removal from water is of great importance because of well-known pesticide resistance to microbial degradation and its ability of accumulation in the environment as well as possible carcinogenic and mutagenic properties [2]. Processes involved in pesticides removal from agricultural waters include chemical oxidation [3–5], Fenton's reaction [6], biological degradation [7], and specially adsorption techniques [8,9].

* Corresponding author. Tel.: +98 611 4457612; fax: +98 611 4435288.

E-mail address: h.tavakkoli@khouzestan.srbiau.ac.ir (H. Tavakkoli).

Among various water purification and recycling technologies, adsorption is a fast, inexpensive and universal method [10]. Many of the studies towards the solution for this problem have been involved determination of adsorptive behavior of pesticides on various adsorbents such as kerolite, Al-pillared clay, bentonite, lignin, quartz, calcite, kaolinite, α -alumina, and activated carbon materials [11–16]. The physical characteristics of the adsorbents such as surface area, porosity, size distribution, density, and surface charge have a major influence on the adsorption process. Thus, efforts have been focused on optimizing adsorption and developing novel alternative adsorbents with high adsorptive capacity. In this regard, more attention has recently been paid to nanotechnology [17,18]. Compared with ordinary sorbents (microsized adsorbents), NPs offer a significantly higher surface area-to-volume ratio and a short diffusion route which results in high extraction capacity, rapid extraction dynamics, and high extraction efficiencies [19,20]. Therefore, satisfactory results can be obtained with fewer amounts of the NPs.

Perovskite-type oxides NPs that were generally formulated as ABO_3 (A is a rare earth metal with large ionic radius or alkali earth metals and B is a transition metal with a small ionic radius) are the novel and promising adsorbents for the adsorption of various analytes such as dyes, volatile organic compounds, pesticides [21–24].

The aim of the present study is to fabricate and characterize two perovskite-type oxide NPs, $\text{LaFe}_x\text{Co}_{(1-x)}\text{O}_3$ ($x = 0.1$ and 0.9) (LFCO1 and LFCO2) and to determine their efficiency in pesticide removal,

Vitavax, from aqueous solutions. For this purpose, the influence of the initial pesticide concentration, adsorbent dosage, temperature, and contact time for adsorption Vitavax on prepared LFCOs NPs was investigated. The kinetic, thermodynamic, and adsorption studies for both LFCOs NPs were done and the results were compared with each other. Based on our knowledge the application of nanoperovskite oxides was investigated for the pesticides removal at the first time in this study.

2. Materials and methods

2.1. Reagents

The chemicals and reagents used in this work include La_2O_3 (99.9%), $\text{Fe}(\text{NO}_3)_3 \cdot 9\text{H}_2\text{O}$ (99.9%) and $\text{Co}(\text{NO}_3)_2 \cdot 6\text{H}_2\text{O}$ (99.9%) obtained from Merck, Germany; citric acid (CA) (99.5% purity), and nitric acid were purchased from Aldrich, USA. All chemicals were analytical grade and used without further purification. The sample solutions were prepared using deionized water throughout the experiments.

5,6-dihydro-2-methyl-N-Phenyl-1,4-oxathiin-3-carboxamide, Vitavax, is a systemic carboxanilide fungicide. Carboxanilide pesticides are used as a seed treatment for control of smut, rots, and blight on corn, and wheat and it has been used against *Rhizoctonia* spp. of vegetables and other diseases. They are used very often in combination with other fungicides such as thiram or captan. Vitavax was supplied by Uniroyal Chemical Company. The used vitavax is the commercial fungicide with 75% wetttable powder, 17% flowable, in combination with carboxin and thiram. The chemical structure, molecular weight, and physical properties of vitavax were given in Table 1.

2.2. Preparation and characterization of the LFCOs NPs

LFCOs NPs of the type perovskite oxide were fabricated by sol-gel method. The appropriate amounts of starting materials $\text{Fe}(\text{NO}_3)_3 \cdot 9\text{H}_2\text{O}$ (99.9%) and $\text{Co}(\text{NO}_3)_2 \cdot 6\text{H}_2\text{O}$ (99.9%) were dissolved in deionized water and La_2O_3 dissolved in nitric acid to form lanthanum nitrate. The aqueous solutions of metal nitrates with nominal atomic ratios La: Fe: Co = 1: 0.9: 0.1 for LFCO1 and La: Fe: Co = 1: 0.1: 0.9 for LFCO2 were mixed together in deionized water. Then, citric acid (CA) was added slowly to the metal solution at room temperature under the constant magnetic stirring (1000 rpm). The solution was concentrated by evaporation at approximately 50 °C with stirring for 1 h to convert it to a stable complex. To make a gel, stirring was continued at ~70 °C for 3 h. The dry gel was obtained by letting the sol into an oven and heated slowly up to 110 °C and kept for 8 h in a baking oven. The gel was ground in an agate mortar and turned into powder. Then, $\text{LaFe}_{0.9}$,

$\text{Co}_{0.1}\text{O}_3$ (LFCO1) and $\text{LaFe}_{0.1}\text{Co}_{0.9}\text{O}_3$ (LFCO2) NPs were obtained by calcination of the precursors at 750 °C for 10 h in air.

The TGA of the gel precursor dried at 110 °C was taken using the Shimadzu50 Thermoanalyzer in the temperature range from 50 to 800 °C (10 °C/min) and a dynamic air atmosphere. The crystal structure of calcined powders at 750 °C were determined by XRD in the region of ($2\theta = 20\text{--}70^\circ$) using $\text{CuK}\alpha$ radiation ($\lambda = 1.5418 \text{ \AA}$) on a Rigaku D/MAX RB XRD diffractometer equipped with a curved graphite monochromator. The FT-IR spectra were taken by using KBr disks method on thermo Nicolet Nexus 870 FT-IR spectrometer. The specific surface areas (SSA) of NPs were measured by applying the BET method over the relative equilibrium pressure of the N_2 adsorption isotherms [25]. The structure and surface morphology of the NPs were studied using SS1 STM and all images were recorded in the constant-current mode at room temperature using a Remanium tip with a bias voltage of around 2 V in atmosphere. The microstructure and elemental distribution on the surface were analyzed by scanning electron microscopy (SEM, LEO 1450 VP, $V = 30 \text{ kV}$) and energy dispersive X-ray spectroscopy (EDX, Inca 400, Oxford Instruments).

2.3. Pesticide removal experiments

Pesticide adsorption by the LFCOs NPs was determined in batch experiments at different contact times (5–40 min), fungicide (vitavax) concentrations (200–800 mg/L), different doses of adsorbent (from 1 to 3 g/L) and various temperatures (15–45 °C). The initial vitavax solution concentration for all batch experiments was adjusted to 200 mg/L except for the experiments in which the effect of the initial vitavax concentration was tested. To get a homogeneous solution, 0.2 g of vitavax was dissolved in 1 L of deionized water and pH value was adjusted using a Metrohm 620 pH meter. A known mass of LFCOs NPs was then added to 10 mL of the vitavax aqueous solution and the obtained suspension was immediately stirred (1000 rpm) and then was centrifuged.

The pesticide concentration was determined by UV-Vis spectrophotometry (Agilent 8453) at λ_{max} 580 nm. The amount of contaminant adsorbed was calculated using the following expression:

$$\text{Removal efficiency \%} = \frac{C_0 - C_e}{C_0} \times 100 \quad (1)$$

where C_0 and C_e are the initial and residual concentrations of vitavax, respectively. All experiments were repeated twice and the mean of the two measurements was reported. All experiments were done at the room temperature except for the experiments that the effect of temperature was examined.

3. Results and discussion

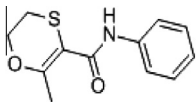
3.1. Characterization of nanoparticles

The xerogels and nanopowders of perovskite-type oxides $\text{LaFe}_x\text{Co}_{(1-x)}\text{O}_3$ with $x = 0.1$ and 0.9 were fabricated by sol-gel method in the presence of citric acid as a chelating agent. The obtained NPs were characterized by TGA, FT-IR, XRD, BET, SEM-EDX, and STM methods.

3.1.1. TGA and FT-IR

Fig. 1 shows the TGA and DTG curves of thermal decomposition process of the $\text{LaFe}_{0.9}\text{Co}_{0.1}\text{O}_3$ (LFCO1) NPs. The total weight loss of the xerogel was approximately 67% and the decomposition process can be divided into three distinct steps. The first weight loss occurred during the heating step from room temperature to 180 °C (24%) resulting from the dehydration and decomposition of nitrates. This is confirmed by the corresponding one weight loss

Table 1
Basic properties of the pesticide.

Characteristic	Pesticide
Type	Organic fungicide
Commercial name	Vitavax
Chemical formula	$\text{C}_{12}\text{H}_{13}\text{NO}_2\text{S}$
Molecular weight (g/mol)	235.3
Melting point (°C)	91.5–92.5
Solubility (mg/L)	170 at 25 °C
λ_{max} (nm)	580
Molecular structure	

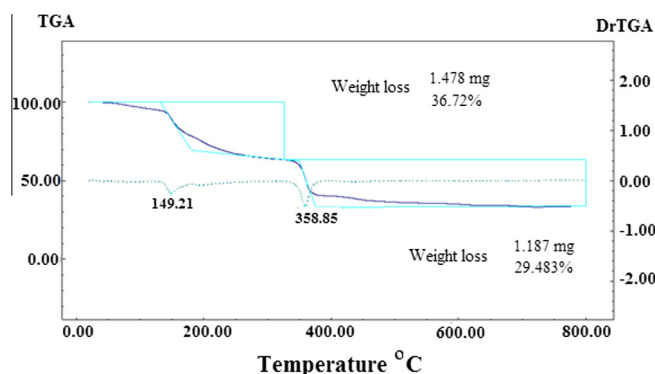


Fig. 1. TGA/DTG curves of the LFCO1 xerogel carried out from room temperature to 800 °C in air.

differential peak (149 °C) in the DTG curve. From 180 °C to about 350 °C, a weight loss of about 13% was observed which attributed to the decomposition of chemically bound groups. The third step from 350 to 650 °C (30%) is due to the oxidation or combustion of the chelate complex along with the forming of metal oxides corresponding to the strongest weight loss differential peak (359 °C) in the DTG curve. No weight loss above 650 °C was detected on the TG curve which indicates the formation of nanocrystalline LFCO as the decomposition product. Hence, it is plausible to conclude that the optimum calcination temperature is about 700 °C.

The FT-IR spectra of the LFCOs fresh xerogel and annealed xerogel in the range of 600–2100 cm^{-1} were shown in Fig. 2. The dried gel of two samples shows the characteristic bands at about 1580 and 1395 cm^{-1} corresponds to the stretching mode of M–O–C group [26,27] and the anti-symmetric NO_3^- stretching vibration [28], respectively. The absorption band around 1070 cm^{-1} is assigned to C–O bond [29]. The bands correspond to O–H group, NO_3^- , and carboxylate impurities disappear as the gel was annealed at 750 °C. This indicates the possibility of metal carboxylate dissociation and conversion to metal oxides during the calcination process.

3.1.2. X-ray diffraction and microscopic analyses

Fig 3 shows the XRD patterns of the LFCOs NPs prepared by sol-gel method and calcined at 750 °C for 10 h. The diffractograms reveal that the crystalline perovskite structure is the main phase for two synthesized solids. The most intense diffraction peak ($2\theta = 32.58$) is a single peak for all of the studied perovskites [30]. The orthorhombic structure of $\text{LaFe}_{0.9}\text{Co}_{0.1}\text{O}_3$ (Fig. 3a) was confirmed by high-intensity peaks with 2θ values 33, 47.4, 58.7 and 68.2. The diffraction peaks for $\text{LaFe}_{0.1}\text{Co}_{0.9}\text{O}_3$ at 2θ of 32.5, 48.3, 59.2 and 69 were doublet, and this pattern was indexed using a rhombohedral unit cell (Fig. 3b) [31]. The crystallite size was calculated using the XRD peak broadening of the ($2\theta = 32$) peak using the Scherer's formula:

$$D_{hkl} = \frac{0.9\lambda}{\beta_{hkl} \cos \theta_{hkl}} \quad (2)$$

where D_{hkl} (nm) is the particle size perpendicular to the normal line of (hkl) plane, λ (nm) is the wavelength of X-ray, β_{hkl} is the full width at half maximum, and θ_{hkl} (Rad) is the Bragg angle of (hkl) peak. The crystallite size of LFCOs-NPs calcinated at 750 °C was about 35 nm.

The morphology and the particle size of LFCOs NPs were studied by SEM and STM methods. Fig. 4 (a: dried xerogel, b and c: calcined xerogel) shows the SEM images for both samples LFCO1 and LFCO2 NPs. As this figure shows LFCO1 NPs are not well-distributed. More than 80% of NPs are at the nano scale and it seems that the NPs were not grown with uniform size. However, the surface looks

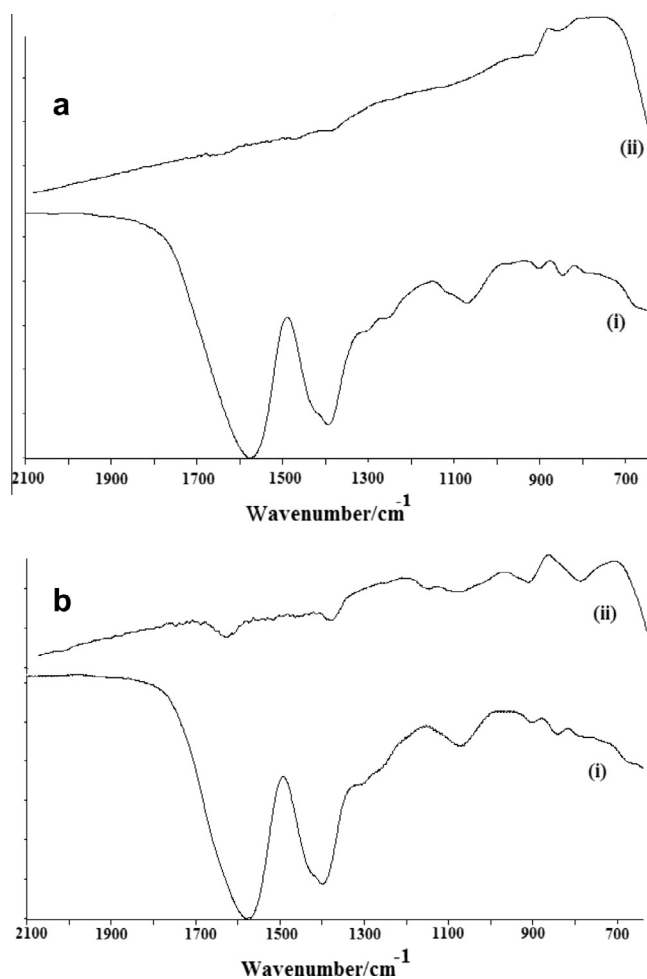


Fig. 2. FTIR spectra of the (a) LFCO1 fresh xerogel (i) the calcined powders at 750 °C (ii) and (b) LFCO2 fresh xerogel (i) the calcined powders at 750 °C (ii).

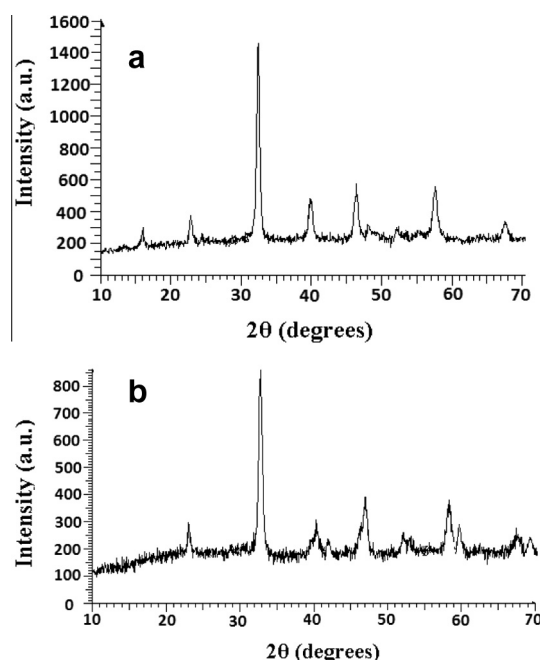


Fig. 3. The XRD patterns of the (a) LFCO1 NPs and (b) LFCO2 NPs calcined at 750 °C.

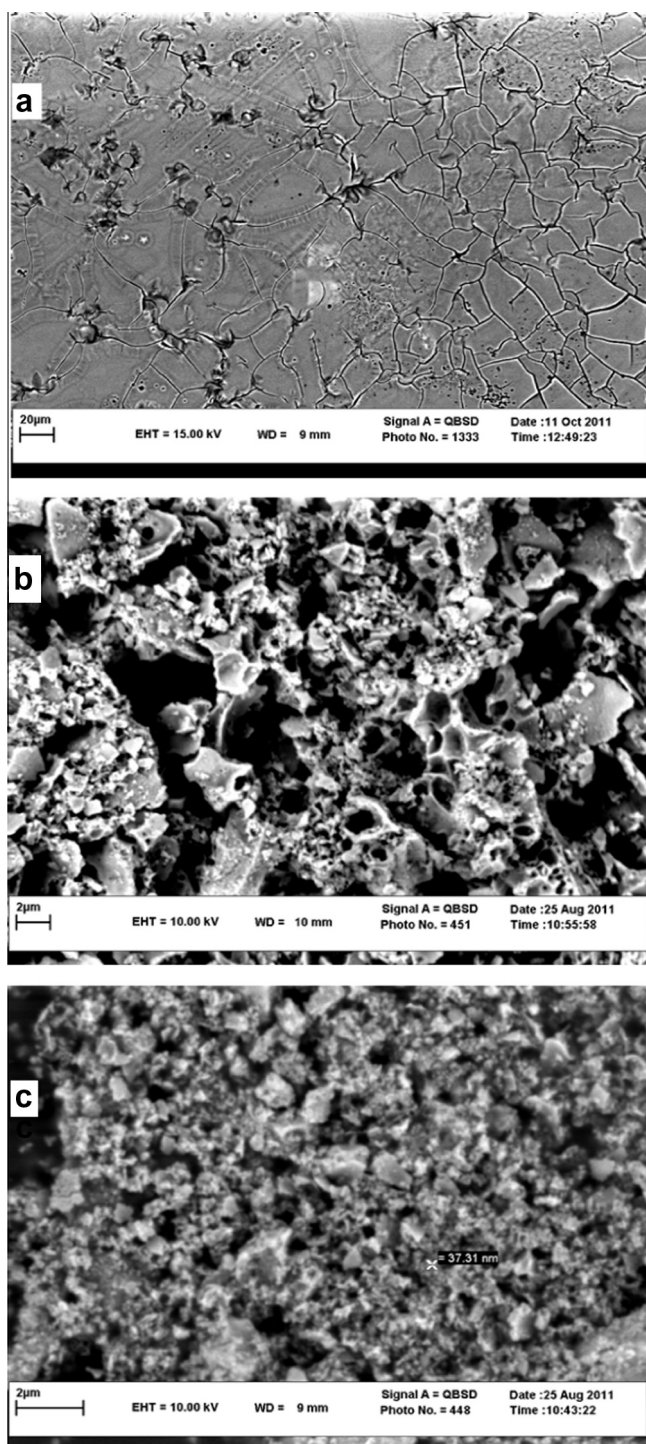


Fig. 4. SEM images for (a) dried xerogel of LFCO1 NPs (b) calcined xerogel of LFCO1 NPs (c) calcined xerogel of LFCO2 NPs.

rough and nearly fully covered with the particles grown on it and the particle size distribution seems to be in the range 50–400 nm. While the grains of LFCO2 sample are nearly spherical with approximately uniform particle size and their distribution is ranging between 30 and 60 nm with the average diameter of about 40 nm.

The EDX analysis attached to SEM was used for further studies of the obtained product composition. Fig. 5 shows the EDX analysis for NPs which confirms the existence of La, Fe, Co, and O elements.

Figs. 6 and 7 show the STM micrographs of LFCO1 and LFCO2 NPs, respectively which can be used to determine the particles size

and height. The bright spots are higher than those of the dark and particles distribution on the surface is mapped obviously. The average particle size and height for LFCO1 NPs were 40 nm and 5 nm, respectively (Fig. 6b). While the average size and height for LFCO2 NPs were found 20 nm and 6 nm, respectively (Fig. 7b).

The BET measurement shows that the SSA of the as-prepared powders for LFCO1 and LFCO2 calcined at 750 °C were 51.2 and 42.8 m²/g, respectively.

3.2. Kinetic study of pesticide removal

The kinetic study of the prepared and characterized LFCO1 NPs as the adsorbents for removal of vitavax from liquid solutions was investigated. The pH of vitavax solution was fixed at 7 for all batch experiments because the vitavax was precipitated in both acidic and basic media.

3.2.1. Effect of adsorbent amounts and contact time

By increasing amounts of LFCO1 NPs, the removal efficiency increased due to increase in the accessible sites for the adsorption of the analyte. Fig. 8 shows that the removal efficiency of vitavax with the initial dosage of 1 g/L increased from 37% to 23% at the fifth minute of contact to 95% and 82% within 40 min under the optimum conditions for LFCO1 and LFCO2 NPs, respectively. However, by increasing LFCO1 dosage to 3 g/L, complete removal (100%) was attained after 25 and 30 min for LFCO1 and LFCO2 NPs, respectively. In addition, increasing the contact time from 5 to 40 min with different dosages of adsorbents led to decreasing in the concentration of vitavax.

3.2.2. Effect of pesticide concentration

The effect of vitavax initial concentrations was studied on the adsorption to LFCO1 powders under the determined optimum conditions (Fig. 9). The removal percentage decreased from 100% with a concentration of 200 mg/L to 58% and 52% with a concentration of 800 mg/L using LFCO1 and LFCO2, respectively. By increasing the initial analyte concentrations, more vitavax is left unadsorbed in the solution due to the saturation of the binding sites. This indicates that energetically less favorable sites become involved with increasing vitavax concentration in aqueous solutions. The equilibrium adsorption capacity of adsorbents was calculated by the following equation:

$$q_e = \frac{V(C_0 - C_e)}{m} \quad (3)$$

where q_e is the equilibrium adsorption capacity of adsorbent in mg vitavax/g adsorbent, V is the volume of vitavax solution in L, and m is the weight of the adsorbent in g. The calculated adsorption capacity of LFCO1 and LFCO2 NPs for the maximum investigated vitavax concentration (800 mg/L) was 155 and 139 mg/g, respectively.

3.2.3. Effect of temperature

The effect of temperature on the vitavax removal onto LFCO1 NPs was carried out at 15, 25, 35 and 45 °C (Fig. 10). Increasing the temperature from 15 to 25 °C led to an increase in the removal efficiency for both adsorbents. Consequently, it is plausible to say that the vitavax adsorption onto these NPs may be a kinetically controlled process. Above 25 °C, increasing the temperature has no important effect on the removal rate at all.

3.3. Adsorption kinetic models

The various kinetic models are available to investigate the adsorption mechanism. The first (Eq. 4) and second order (Eq. 5) reaction rate equations are the most commonly applied models:

$$\ln C(t) = \ln C_0 - k_1 t \quad (4)$$

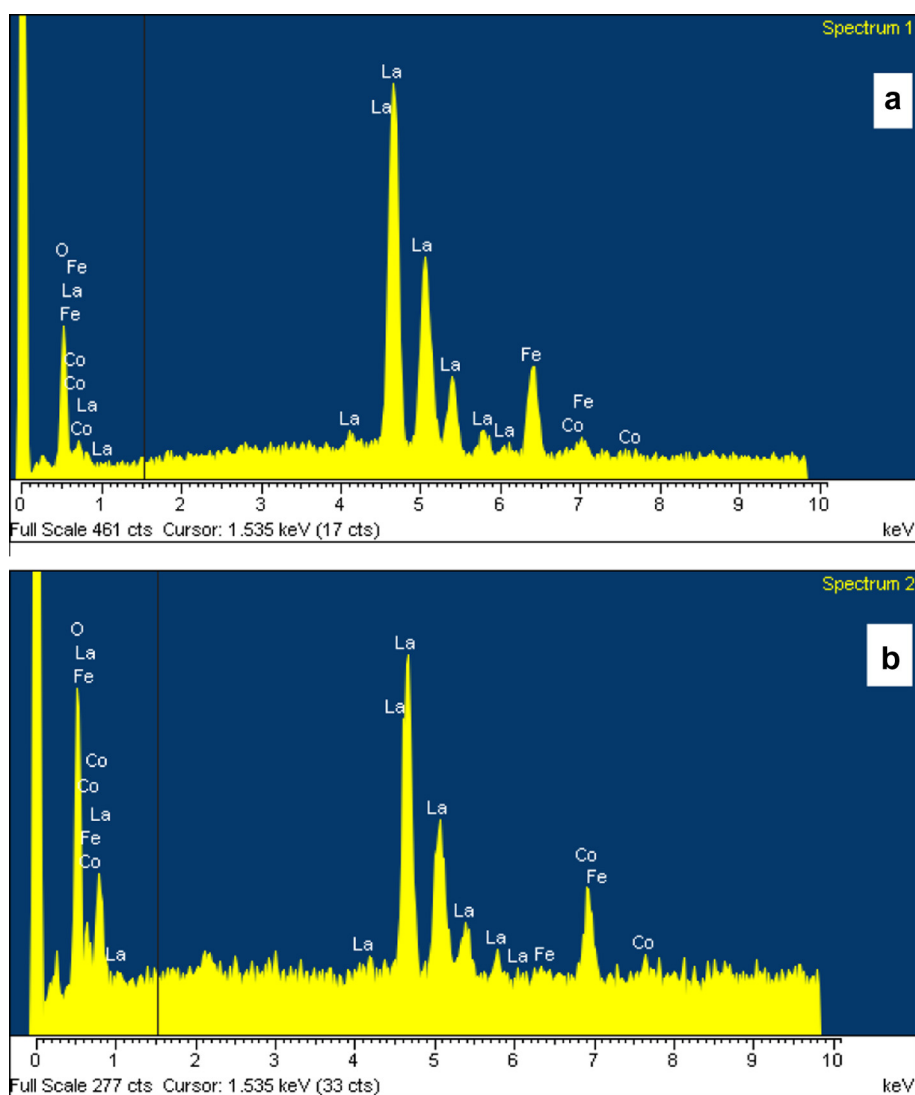


Fig. 5. Result of EDX analysis of the (a) LFCO1 and (b) LFCO2 NPs.

$$\frac{1}{C(t)} = k_1 t + \frac{1}{C_0} \quad (5)$$

where k_1 and k_2 are the first-order and second-order rate constants, respectively; $C(t)$ is the concentration of vitavax at time t . Table 2 gives a summary of the kinetic study of vitavax adsorption by NPs. As the table shows the removal of vitavax by the NPs obeys the first-order kinetic model by referring the values of correlation coefficients (R^2).

To determine the activation energy, E_a , of the adsorption process, the well-known Arrhenius equation was employed. The values of activation energy and the pre-exponential factor was 7.6 kJ mol^{-1} and 1.4 min^{-1} for LFCO1 NPs, and 4.37 kJ mol^{-1} and 0.22 min^{-1} for LFCO2 NPs, respectively.

3.4. Adsorption isotherm models

The equilibrium adsorption isotherm is fundamental in describing the interactive behavior between solutes and adsorbent and it is important for the design of an adsorption system. Several isotherm models such as Langmuir, Freundlich, and Redlich–Peterson have been used to explain the nonlinear equilibrium relationship between the solute adsorbed onto the adsorbent and that left in the solution. In this work, two common adsorption isotherm models of Langmuir and Freundlich [32,33] were used to study the adsorption data. The linear form of the Langmuir isotherm is defined by:

$$\frac{C_e}{q_e} = \frac{1}{b q_{\max}} + \frac{C_e}{q_{\max}} \quad (6)$$

where the q_{\max} (mg/g) is the surface concentration at monolayer coverage which illustrates the maximum value of q_e and it can be attained as C_e is increased. The b parameter is the Langmuir adsorption equilibrium constant which is relates to the energy of adsorption. The values of q_{\max} and b can be determined from the linear regression plot of (C_e/q_e) versus C_e .

The linear form of the Freundlich isotherm is expressed as follows:

$$\log q_e = \log K_F + \frac{1}{n} \log C_e \quad (7)$$

where K_F and n are constants of the Freundlich equation. The constant K_F represents the capacity of the adsorbent for the adsorbate and n relates to the adsorption distribution. A linear regression plot of $\log q_e$ versus $\log C_e$ gives the K_F and n values.

Table 3 summarizes the constants of both isotherms and the corresponding correlation coefficients. The value of the correlation coefficients of the Langmuir isotherm was greater than that of the Freundlich isotherm. This indicates that the adsorption of vitavax on LFCO1 and LFCO2 NPs is better described by the Langmuir model.

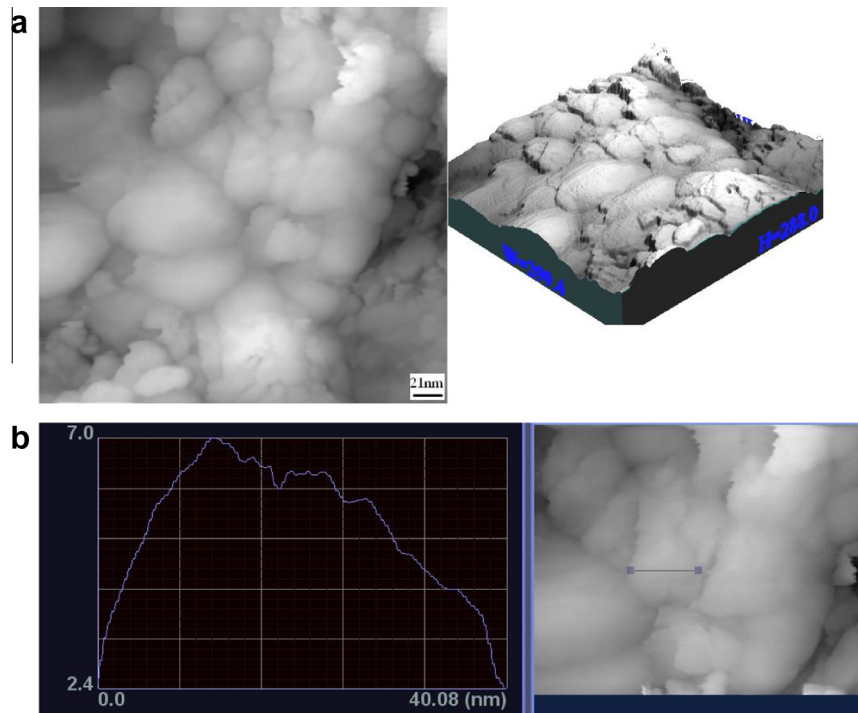


Fig. 6. (a) STM images of LFCO1 NPs for the area of 30×300 nm, (b) height profile along the white line.

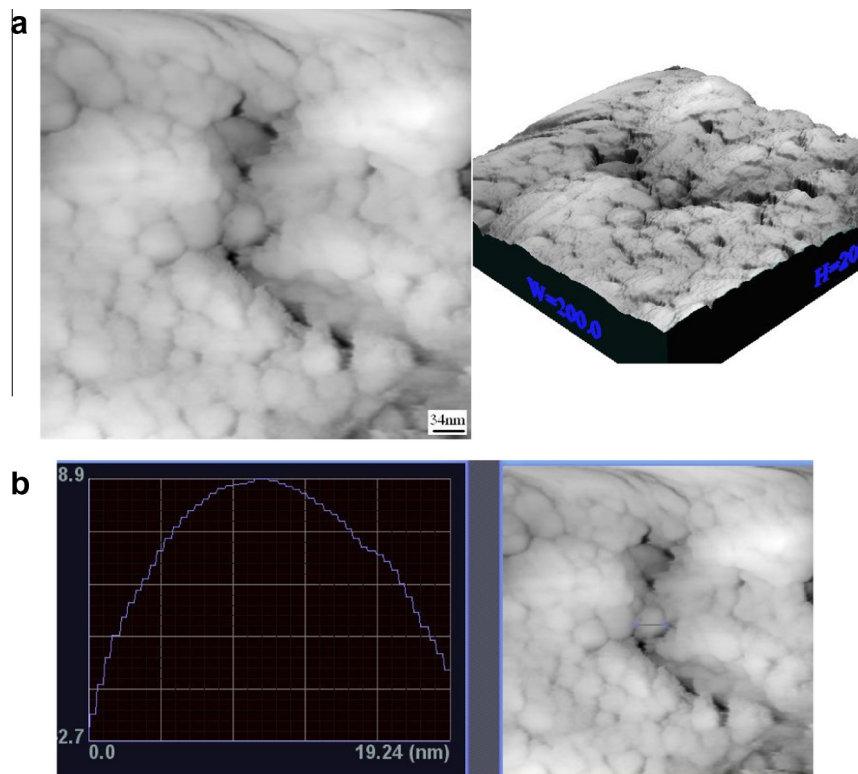


Fig. 7. (a) STM images of LFCO2 NPs for the area of 200×200 nm, (b) height profile along the white line.

The essential characteristics and the feasibility of the Langmuir isotherm is described in terms of a dimensionless constant separation factor (R_L) [34]:

$$R_L = \frac{1}{1 + bC_0} \quad (8)$$

The R_L value indicates the shape of the isotherm as follows: irreversible ($R_L = 0$), favorable ($0 < R_L < 1$), linear ($R_L = 1$), or unfavorable ($R_L > 1$). The R_L values for the adsorption on LFCO1 and LFCO2 NPs fall between 0 and 1; hence, the adsorption is a favorable process.

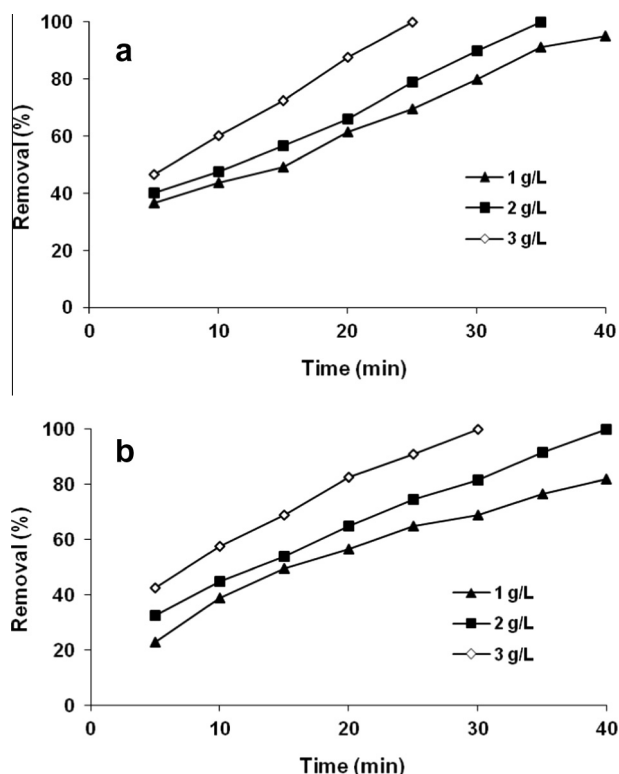


Fig. 8. Effect of stirring time on removal of vitavax in different doses of (a) LFCO1 NPs (b) LFCO2 NPs. Experimental Conditions: initial pesticide concentration = 200 mg/L, initial pH 7, temperature = 25 °C.

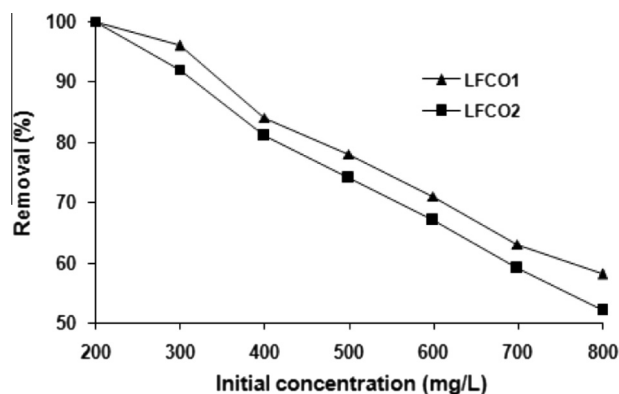


Fig. 9. Effect of initial pesticide concentration on removal of vitavax. Experimental Conditions: LFCOs-NPs dosage = 3 g/L, initial pH 7, stirring time = 30 min, temperature = 25 °C.

3.5. Adsorption thermodynamics

The thermodynamic parameters, the standard Gibbs energy change, ΔG° , the standard enthalpy change, ΔH° , and the standard entropy change, ΔS° , were calculated using the experimental data obtained at various temperatures by the following equations.

$$\Delta G^\circ = -RT \ln Ke \quad (9)$$

$$\ln Ke = -\left(\frac{1}{RT}\right)\Delta H^\circ + C \quad (10)$$

$$\Delta S^\circ = \frac{\Delta H^\circ - \Delta G^\circ}{T} \quad (11)$$

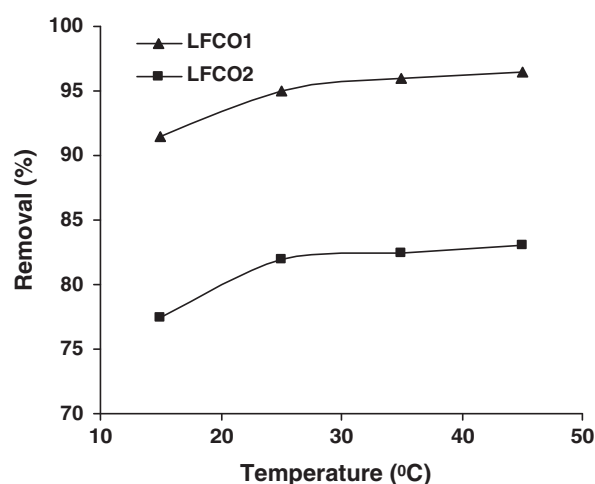


Fig. 10. Effect of temperature on removal of vitavax. Experimental Conditions: LFCOs-NPs dosage = 1 g/L, initial pesticide concentration = 200 mg/L, initial pH 7, stirring time = 40 min.

Table 2

Adsorption kinetic study for removal of vitavax by the NPs.

Adsorbent	$q_{e,exp}$	First-order model		Second-order model	
		K_1 (min^{-1})	R^2	K_2 ($\text{mg}^{-1} \text{L min}^{-1}$)	R^2
LFCO1	155	0.07	0.971	0.002	0.69
LFCO2	139	0.04	0.993	0.001	0.92

where K_e is equilibrium constant which can be calculated by plotting $\ln(q_e/C_e)$ versus q_e and extrapolating to zero q_e . R is the universal gas constant ($8.314 \text{ JK}^{-1} \text{ mol}^{-1}$) and C is a constant. Table 4 shows the thermodynamic parameters of the vitavax onto the NPs. The negative values of the standard Gibbs free energy at various temperatures indicate the spontaneous nature of the adsorption of vitavax from aqueous solutions by LFCOs NPs [35]. The positive values of the standard enthalpy suggest the adsorption is an endothermic process. The positive values of standard entropy change reflect the increasing randomness at the solid/liquid interface during the adsorption of vitavax on the NPs.

4. Conclusions

The LFCO1 and LFCO2 NPs namely $\text{LaFe}_{0.9}\text{Co}_{0.1}\text{O}_3$ and $\text{LaFe}_{0.1}\text{Co}_{0.9}\text{O}_3$ were prepared by the sol-gel method and heat treatment at 750 °C. Systematic studies were carried out to characterize and examine the structural, morphological, and removal pesticide efficiency of LFCOs NPs. The XRD patterns reveal that the LFCOs NPs have good crystallinity with orthorhombic and hexagonal structure for LFCO1 and LFCO2, respectively. The SEM and STM images show regular morphology and particle size distribution on the surface. The FTIR spectroscopy also confirmed the structure of obtained NPs.

The present study showed that the prepared NPs are efficient adsorbents of vitavax fungicide in a short time. In addition, it was found that the percentage of removal of vitavax by LFCO2 NPs is less than that for LFCO1 NPs at the same conditions. The kinetic study revealed that the first-order kinetic model describes the removal process of vitavax onto the NPs. Also, the adsorption obeyed the Langmuir isotherm. Thermodynamic study indicates that the adsorption of vitavax is feasible, and spontaneous in nature.

Table 3
Adsorption isotherms parameters of vitavax.

Adsorbent	Langmuir model			Freundlich model		
	q_{max} (mg g ⁻¹)	b (L mg ⁻¹)	R^2	K_f (mg ^{1-1/n} L ^{1/n} g ⁻¹)	n	R^2
LFCO1	166.67	0.070	0.994	67.92	7.41	0.904
LFCO2	142.86	0.076	0.997	66.52	8.47	0.848

Table 4
Thermodynamic parameters for removal of vitavax.

T (°C)	LFCO1			LFCO2		
	$-\Delta G^\circ$ (kJ mol ⁻¹)	ΔH° (kJ mol ⁻¹)	ΔS° (J mol ⁻¹ K ⁻¹)	$-\Delta G^\circ$ (kJ mol ⁻¹)	ΔH° (kJ mol ⁻¹)	ΔS° (J mol ⁻¹ K ⁻¹)
15	2.87	20.76	82.00	3.07	23.29	91.49
25	5.23		87.17	5.33		96.00
35	5.46		85.10	5.94		94.89
45	5.77		83.28	6.24		92.84

Table 5
Comparison of the experimental conditions and removal efficiency of some pesticides via different adsorbents.

Pesticide type	Adsorbent type	Pesticide concentration (mg/L)	Adsorbent dosage (g/L)	Contact time (min)	Percentage removal (%)	References	
Isoproturon (IPU)	Powdered activated charcoal	1.0	0.3-1.0	120	98–99	[36]	
Bromopropylate (BP)	bentonite	2.5	5	135	90–100	[37]	
	chitosan			75			
	Corn cob			135			
	Olive kernels			135			
Ametryn	Activated carbon-cloth	103.8	0.9	125	85	[38]	
					Aldicarb		34
					Dinoseb		87
					Diuron		49
α -Endosulphan	Activated carbon	5.0×10^{-4}	–	–	80	[39]	
					Parathion methyl		80
					Atrazine		55
					Prometryn		60
Methoxychlor, Methyl parathion, Atrazine	Waste rubber tire	12.0	0.14	150	95	[8]	
					73		
					87.5		
					95		
Vitavax	Nano perovskite LFCO1	200	1.0	40	95	This work	
			2.0	35	100		
			3.0	25	100		
			3.0	30	100		
Vitavax	Nano perovskite LFCO2	200	1.0	40	82		
			2.0	40	100		
			3.0	30	100		

A comparison of the experimental conditions and removal efficiency of some pesticides via different adsorbents is given in Table 5. The results indicate that the proposed synthesized adsorbents are superior to the reported ones. One of the most features of this study is that the contact time for complete removal of vitavax by LFCOs NPs is less than that of other adsorbents.

Acknowledgments

This work was funded by Ferdowsi University of Mashhad under the project of P439. The authors are grateful to Dr. E. K. Goharshadi for her help and acknowledge the Central Laboratory Unit of Ferdowsi University for taking SEM and STM images and EDX analysis.

References

[1] S. Dasgupta, C. Meisner, D. Wheeler, *J. Environ. Manage.* 91 (2010) 824–830.
 [2] D.L. Becker, S.C. Wilson, *Carbon Adsorption Handbook*, in: P.N. Cheremisinoff, F. Ellebush (Eds.), The use of activated carbon for the treatment of pesticides and pesticidal wastes, Ann Harbor Science Publishers, Michigan, 1980.
 [3] J.P. Scott, D.F. Ollis, *Environ. Prog.* 14 (1995) 88–103.
 [4] P.L. Huston, J.J. Pignatello, *Environ. Sci. Technol.* 30 (1996) 3457–3463.
 [5] J. Prousek, *Chem. Listy* 90 (1996) 229–237.
 [6] K. Barbusiński, K. Filipek, *Pol. J. Environ. Stud.* 10 (2001) 207–212.
 [7] G. Yanez-Ocampo, E. Sanchez-Salinas, M.L. Ortiz-Hernandez, *Biodegradation* 22 (2011) 1203–1213.
 [8] V.K. Gupta, B. Gupta, A. Rastogi, S. Agarwal, A. Nayak, *Water Res.* 45 (2011) 4047–4055.
 [9] S. Kushwaha, G. Sreelatha, P. Padmaja, *J. Chem. Eng. Data* 56 (2011) 2407–2415.
 [10] I. Ali, V.K. Gupta, *Nat. Protoc.* 1 (2007) 2661–2667.
 [11] E. Gonzalez-Pradas, M. Socias-Viciano, M. Saifi, M.D. Urena-Amate, F. Flores-Cespedes, M. Fernandez-Perez, M. Villafranca-Sanchez, *Chemosphere* 51 (2003) 85–93.
 [12] I.K. Konstantinou, T.A. Albanis, D.E. Petrakis, P.J. Pomonis, *Water Res.* 34 (2000) 3123–3136.
 [13] E. Bojemueller, A. Nennemann, G. Lagaly, *Appl. Clay Sci.* 18 (2001) 277–284.
 [14] J. Ludvik, P. Zuman, *Microchem. J.* 64 (2000) 15–20.
 [15] L. Clausen, I. Fabricius, L. Madsen, *J. Environ. Qual.* 30 (2001) 846–857.
 [16] S. Sadasivam, S.K. Krishna, K. Ponnusamy, G.S. Nagarajan, T.W. Kang, S.C. Venkatesalu, *J. Chem. Eng. Data* 55 (2010) 5658–5662.
 [17] B. Van der Bruggen, J. Schaep, W. Maes, D. Wilms, C. Vandecasteele, *Desalination* 117 (1998) 139–147.
 [18] M. Yazdanbakhsh, I. Khosravi, E.K. Goharshadi, A. Youssefi, *J. Hazard. Mater.* 184 (2010) 684–689.
 [19] A. Afkhami, R. Moosavi, *J. Hazard. Mater.* 174 (2010) 398–403.

- [20] V.K. Gupta, B. Gupta, A. Rastogi, S. Agarwal, A. Nayak, *J. Hazard. Mater.* 186 (2011) 891–901.
- [21] S. Songa, L. Xua, Z. Hea, H. Ying, J. Chena, X. Xiao, B. Yan, *J. Hazard. Mater.* 152 (2008) 1301–1308.
- [22] M. Yazdanbakhsh, H. Tavakkoli, S.M. Hosseini, *Desalination* 281 (2011) 388–395.
- [23] J. Niu, J. Deng, W. Liu, L. Zhang, G. Wang, H. Dai, H. He, X. Zi, *Catal. Today* 126 (2007) 420–429.
- [24] S. Devipriya, S. Yesodharan, *Sol. Energy Mater. Sol. Cells* 86 (2005) 309–348.
- [25] S. Brunauer, P.H. Emmet, E. Teller, *J. Am. Chem. Soc.* 60 (1938) 309–319.
- [26] P.N. Kuznetsov, L.I. Kuznetzova, A.M. Zhyzhaev, G.L. Pashkov, V.V. Boldyrev, *Appl. Catal. A* 227 (2002) 299–307.
- [27] J. Kim, I. Honma, *Electrochim. Acta* 49 (2004) 3179–3183.
- [28] S. Liu, X. Qian, J. Xiao, *J. Sol–Gel Sci. Technol.* 44 (2007) 187–193.
- [29] K. Nakamoto, *Infrared and Raman Spectra of Inorganic and Coordination Compounds*, Plenum Press, New York, 1978.
- [30] N.A. Merino, B.P. Barbero, P. Ruiz, L.E. Cadus, *J. Catal.* 240 (2006) 245–257.
- [31] F. Bin, C. Song, G. Lv, J. Song, C. Gong, Q. Huang, *Ind. Eng. Chem. Res* 50 (2011) 6660–6667.
- [32] I. Langmuir, *J. Am. Chem. Soc.* 40 (1918) 1361–1403.
- [33] H. Freundlich, W. Heller, *J. Am. Chem. Soc.* 61 (1939) 2228–2230.
- [34] G. Mckay, H.S. Blair, J.R. Gardener, *J. Appl. Polym. Sci.* 27 (1982) 3043–3057.
- [35] M. Akhtar, S.M. Hasany, M.I. Bhangar, S. Iqbal, *Chemosphere* 66 (2007) 1829–1838.
- [36] B. Sarkara, N. Venkateswralub, R. Nageswara Raob, C. Bhattacharjee, V. Kalea, *Desalination* 212 (2007) 129–140.
- [37] O.A. Ioannidou, A.A. Zabaniotou, G.G. Stavropoulos, M.A. Islam, T.A. Albanis, *Chemosphere* 80 (2010) 1328–1336.
- [38] E. Ayranci, N. Hoda, *Chemosphere* 60 (2005) 1600–1607.
- [39] M.P. Ormad, N. Miguel, A. Claver, J.M. Matesanz, J.L. Ovelleiro, *Chemosphere* 71 (2008) 97–106.